Theor Chem Acc (2007) 117:663–671
DOI 10.1007/s00214-006-0191-4

REGULAR ARTICLE

Chemistry *of* and *on* TiO_2-anatase surfaces by DFT calculations: a partial review

Andrea Vittadini · Maurizio Casarin · Annabella Selloni

Received: 12 September 2006 / Accepted: 10 October 2006 / Published online: 8 December 2006

Abstract We review recent theoretical studies of the surfaces and interfaces of the anatase polymorph of TiO_2. We discuss aspects of the surface structure, stability, and reactivity, as well as the growth and stability of anatase-supported oxide nanostructures of catalytic interest. Finally, we report on recent investigations of two-dimensional titania systems which appear to be closely related to anatase and which may have an important role during the growth of anatase nanoparticles.

Keywords Titanium dioxide · Anatase · Surfaces · Adsorption · Nanolayers · Density functional calculations

1 Introduction

Titanium dioxide stands as one of the most important metal oxides for technological applications [1]. The most stable polymorph is rutile [2], but anatase and brookite are also common, especially in nanoscale natural and synthetic samples. In particular, anatase is very interesting because of its activity in catalysis and photocatalysis [1,3,4]. However, the difficulties of obtaining anatase samples of good quality has limited for a long time the degree of understanding of the surface properties and reactivity of this material. As Madey pointed out in the concluding remarks of the Faraday Discussions conference held in Ambleside (1999) [5], almost all attention at that time was devoted to the better-characterized rutile surfaces. Since then, increasing synthetic, experimental, and theoretical efforts have helped to clarify several aspects of the surface chemistry of anatase. As indicated in the title, the present paper is not intended to give an exhaustive review of the available theoretical work on anatase. Our aim is rather to focus on what we believe to be quite interesting aspects of this material, mainly making reference to our research activity over the last 10 years.

2 Computational details

The calculations described in this paper were performed on periodically repeated slab models. We used density functional theory (DFT)-based plane-wave pseudopotential total-energy and Car–Parrinello [6] codes which have been recently merged in the Quantum Espresso distribution [7]. The basic computational settings, which are common to all the calculations, include small core Vanderbilt pseudopotentials [8], 25 Ry kinetic energy cutoff for the plane waves, and 200 Ry cutoff for the augmented density. For a complete description of the computational parameters, however, the reader is referred to the original papers, as several details (optimization scheme, *k*-point sampling of the Brillouin zone, exchange-correlation functional, etc.) depend on the specific system under investigation.

A. Vittadini (✉)
ISTM-CNR, Dipartimento di Scienze Chimiche (DiSC), Università di Padova, via Marzolo 1, 35131 Padova, Italy
e-mail: andrea.vittadini@unipd.it

M. Casarin
Dipartimento di Scienze Chimiche, Università di Padova, via Marzolo 1, 35131 Padova, Italy

A. Selloni
Chemistry Department, Princeton University, Princeton, NJ 08554, USA

Table 1 PBE surface energies for low-index anatase surfaces computed for unrelaxed (E^{unr}) and relaxed (E^{rel}) structures. Values are in J/m^2 (after Ref. [9])

Surface	(101)	(100)	(001)	(110)
E^{unr}	1.28	1.59	1.12	2.17
E^{rel}	0.49	0.58	0.98	1.15

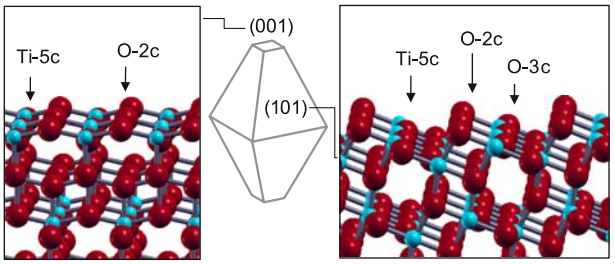

Fig. 1 Equilibrium shape of the anatase crystal (after Ref. [9]). The atomic structures of the minority (001), *left*, and the majority (101) surfaces are also shown. *Blue* and *red spheres* are Ti and O ions, respectively

3 Anatase bulk phase and clean surfaces

The structural properties of the bulk phase and of the low-index surfaces of the anatase and rutile polymorphs of TiO_2 were studied in Ref. [9] using the PBE, the LDA, and the BLYP functionals. The structural and elastic properties were computed for both polymorphs, and found to be in excellent agreement with the experiment. The surface energies of the (101), (100), (001), and (110) surfaces of anatase were also computed, see Table 1. It appears that (i) the (101) is the most stable surface, consistent with the experimental evidence,[1] (ii) relaxation greatly lowers the energy of all surfaces but the (001) one. In spite of this, the unstable (001) surface is expected to be present as a minority surface in most anatase (nano)crystals, as the Wulff construction [12] obtained from the computed surface energies yields a truncated bipyramid, where the main faces consist of {101} planes, while the bases are {001} faces (see Fig. 1). For this reason, we will focus our attention on the (101) and (001) surfaces in the following (for a recent review addressing also other surfaces, see Ref. [13]).

It is useful to give a brief description of the atomic structure of these two surfaces. On the (001) surface (see Fig. 1, left), only twofold coordinated O ions (O-2c), and fivefold coordinated cations (Ti-5c) are present. In contrast, the (101) surface (see Fig. 1, right) also exposes atomic species in a bulk-like coordination, i.e. threefold coordinated O ions (O-3c) and sixfold coordinated Ti ions (Ti-6c). However, these ions do not influence significantly the surface reactivity. Since the (101) surface is the most abundant one, one may expect that the chemistry of anatase will be largely determined by this surface. From a chemical point of view, however, stability implies low reactivity. This suggests that, to predict the *reactivity* of anatase nanocrystals, the minority (001) surfaces, as well as defects (viz. anion vacancies and steps) of the (101) majority surface, could play an important or even leading role.

[1] Actually, calculations by Beltrán et al. [10] predicted the (001) surface to be most stable, but this also contrasts both with subsequent calculations [11] and with the experiment [1].

4 Reactivity of anatase surfaces

Understanding the effects of water adsorption is of uttermost importance, as water is a required ingredient for several growth processes, and the presence of water is also common in the operating conditions of anatase-based devices, e.g. in dye-sensitized solar cells. Already several years ago, we predicted that whereas water adsorption on the (101) surface yields weakly bound ($E_{ads} \sim 0.7$ eV) molecular species, adsorption of water on the (001) surface gives rise to a much stronger interaction ($E_{ads} \sim 1.4 - 1.6$ eV) [14]. Furthermore, whereas the (101) surface structure is not perturbed by the adsorbate, which, in turn, maintains its molecular form, the (001) surface undergoes a major restructuring: water dissociates, disrupting one of the bonds of the bridging oxygens (see Fig. 2, left). These calculations have been recently revisited by other researchers [15,16], who also examined the effects of water on the equilibrium crystal morphology as obtained from Wulff plots (see Sect. 3).

The reasons of the high reactivity of the bridging oxygens on the (001) surface were explained by Lazzeri et al. [17], who noticed that the (001) surface is under tensile stress, due to the unnatural geometrical configuration of the bridging oxygen. On the clean surface, the tensile stress is eliminated by partially replacing the arrays of bridging oxygens with a TiO_2 polymeric structure made of tetrahedrally coordinated Ti atoms, which gives rise to a (1×4) reconstruction. This shortens the Ti–O bonds to 1.8 Å, and closes the Ti–O–Ti angle from ~150 to ~120 degrees, a value which is stereochemically more appropriate for a twofold coordinated O species. Apparently (see Fig. 2), the geometry changes undergone by the (001) surface upon reconstruction and water adsorption are very similar, which means that the tensile stress largely determines the chemistry of this surface.

The stronger reactivity of the minority (001) surface with respect to the majority (101) one is confirmed by investigations of the adsorption of formic acid

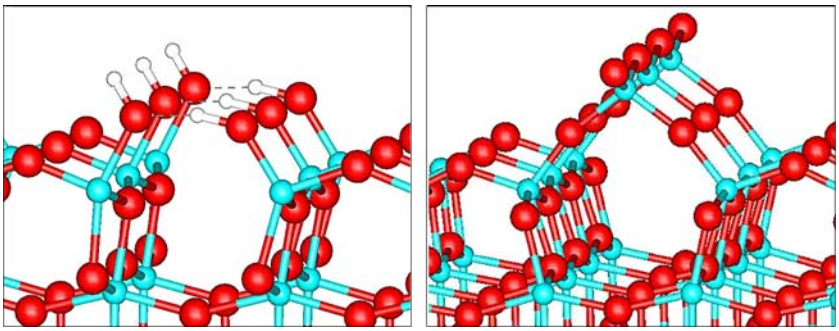

Fig. 2 Atomic structures of a (001) surface covered by 0.5 ML of water (*left*) [14], and of the region close to the ridge of "added molecule" model of the (1 × 4)-reconstructed clean (001) surface (*right*) [17]

(HCOOH). Detailed information on HCOOH adsorption is very valuable, because HCOOH is the simplest organic acid, i.e. the simplest species carrying a carboxylate group, which is used to anchor the "N3" dyes in anatase-based solar cells [3]. Calculations show that on the (101) surface HCOOH remains undissociated, and it is coordinated in a monodentate geometry to a fivefold Ti cation [18], simultaneously interacting through the OH group with a neighboring O(2c) ion. This configuration seems to be generally preferred by acidic species of medium strength, and it has recently predicted to occur also for phosphonic acid [19], and for pyridine phosphonic acid and isonicotinic acid [20]. In contrast, HCOOH adsorbs dissociatively on the (001) surface, where it forms a bidentate-bridging configuration [21]. The HCOOH adsorption energies (0.9 and 1.7 eV on the (101) and (001) surfaces, respectively) are ∼0.2 eV higher than those of water, which means that HCOOH is able to replace water adsorbed at the anatase surface. In line with its considerable stability, the (101) surface exhibits a rather low basicity: in order to observe dissociation, we have to consider a very strong acid as HI [22].

In addition, the adsorption energies of several Lewis bases on the (101) surface have been computed, including CO (0.17 eV [23]), H_2S (0.49 eV [22]), CH_3OH (0.75 eV [24]), NH_3 (0.92 eV [25]). It should be noticed that the energy order does not closely follow the trend of the gas-phase proton affinites [26], because the adsorbate molecules can simultaneously interact both with the Ti(5c) Lewis acid center and with the O(2c) Lewis basic center. Thus, H_2O and CH_3OH can be stabilized by the formation of hydrogen bonds.

The influence of defects, such as oxygen vacancies, on the surface reactivity is an important issue in the chemistry of oxide surfaces. Although anatase is known to be less defective than rutile [27], the presence of even a tiny amount of vacancies can be very important for the reactivity of a substantially inert surface as the (101) one (see also Sect. 6). Tilocca and Selloni found that water dissociatively adsorbs at vacancies, with an activated process that does not follow a direct pathway [28]. The interaction of methanol with vacancies or with hydroxyls formed by water dissociation at vacancies has also been studied [24]. Similarly to water, methanol dissociates at vacancies, whereas molecular and dissociative adsorption are competitive when hydroxyls are introduced.

Turning next to the (001) surface, since the clean, unreconstructed surface is actually unlikely to exist, it makes sense to consider the reactivity of either the hydroxylated surface, which is stable also after evacuation, or the (1 × 4)-reconstructed one, which can be obtained under controlled conditions in UHV. Molecules adsorbed on the hydroxylated (001) surface can be considered as a sort of second-layer adsorbates, and interact most effectively with the hydroxyl group pointing out of the surface. However, secondary interactions with the surface are able to influence adsorption energies (∼ 0.8 eV [14] for H_2O, to be compared to 0.68 eV for NH_3 [25]).

Not much is known about the chemistry of the reconstructed (001)–(1 × 4) surface. Recent work [21] has found that whereas the terrace atoms are almost inert, the ridge ones are very reactive. Similarly to what happens on the unreconstructed surface, the O-bridges of the ridge are partially disrupted upon water exposure (see Fig. 3), and the H_2O adsorption energy is even higher (1.82 eV) than on the unreconstructed surface. Formic acid also reacts very strongly with the ridge atoms, giving rise to several local minima. The most stable structures are a monodentate species, in a configuration similar to that assumed by water (Fig. 3, center), and a bidentate chelating species (Fig. 3, right). Although the bidentate chelating species is predicted to be more stable than the monodentate one (2.15 vs. 1.66 eV), a comparison of the computed Local Density Of States with experimental Scanning Tunneling Microscopy (STM) images [29] indicates that the monodentate species is actually present in UHV adsorption experiments. Thus, a substantial kinetic barrier must occur for the formation of the bidentate-bridging species.

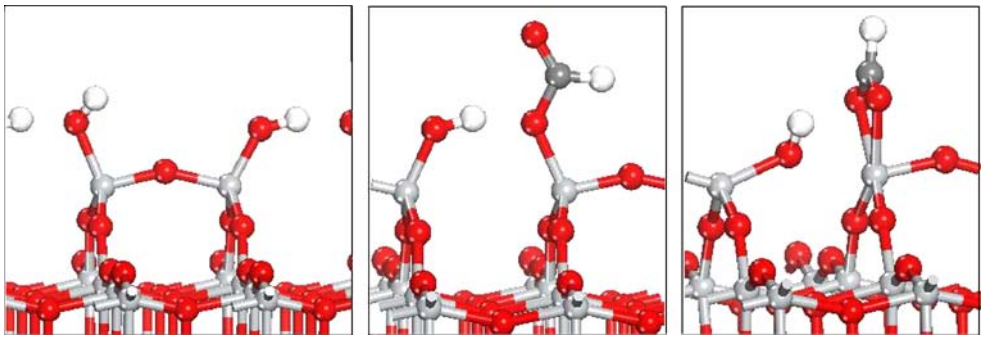

Fig. 3 Adsorption at the ridge of the (1 × 4)-reconstructed (001) surface. Displayed configurations are dissociatively adsorbed water (*left*), and dissociatively adsorbed HCOOH, in a monodentate (*center*) and bidentate (*right*) configuration (after Ref. [21])

5 Anatase as a support

Titania is widely used as a support for catalysts. In this field, however, the degree of the understanding is often poor not only for the mechanism of the catalytic process, but also for the structure of the active layer. The reasons of the different performance of anatase- and rutile-supported catalysts are also unclear. In such a situation, theoretical modeling can be very useful in providing information on the basic atomic scale processes.

In the attempt to gain insight into the growth mechanism of titania-supported metal catalysts, a few years ago we studied the interaction of small gold clusters with stoichiometric and reduced anatase (101) surfaces [23]. We found that on the stoichiometric surface, the cluster–surface interaction is rather weak, so that clusters tend not to wet the surface (see Fig. 4), and the clusters are weakly perturbed when adsorbed. This tendency seems to be a rather general feature of the (101) surface, since very recently a similar behavior has been also predicted for Pt clusters [30]. This picture, however, changes substantially when surface oxygen vacancies are present: the adsorption energies increase, and clusters tend to wet the surface.

Another important class of titania-supported catalysts is VO_x/TiO_2. This system is active in a number of chemical processes, as the selective catalytic reduction of NO [31], the *o*-xylene oxidation to phthalic anhydride [32], and methanol oxidation [33]. On the industrial scale, these catalysts are prepared by impregnating the support with a concentrated solution of a vanadium salt, such as NH_4VO_3. A calcination treatment at high temperature is finally applied. The resulting catalyst contains several vanadia phases, which are believed to be a thin layer (possibly a monolayer) tightly bound to the support, an amorphous vanadium oxide phase, and, for high loadings, vanadia crystallites [32]. Work made on model catalysts [34,35] suggests that the main mechanism allowing the formation of the vanadia "monolayer" is the reaction of the vanadium molecular species with the hydroxyls carried by the support surface. Experimentally, such species are used through "grafting" techniques, where molecular precursors like $VOCl_3$ or $VO(OR)_3$ are allowed to selectively react with surface hydroxyls. These studies revealed that initial vanadia species have a tetrahedral structure, which does not seem to fit models where VO_x species are obtained by perturbing a V_2O_5 structure [36]. Results described in Sect. 3 suggest that grafting of vanadia precursors should occur especially on the (001) surface, where hydroxyls are predicted to be most abundant. On this basis, we explored the stability of several possible structure of "VO_x" species which can be ideally obtained by formally condensing a $VO(OH)_3$ model precursor with the (001) surface hydroxyls groups[2] [37]. In close agreement with the experimental evidence [34], the most stable species turn out to be two tetrahedrally structured units, which are sketched in Fig. 5. The species formed by a single V atom ("monomer") carries a hydroxy and a terminal oxo group, whereas the species formed by two V atoms carries a bridging oxygen and two terminal oxo groups. The latter species ("dimer") can be formally obtained by the condensation of two monomers. It may be noted that both the monomer and the dimer structures are closely related to the tetrahedrally structured TiO_2 polymers of the "added molecule" model of the (1 × 4)-reconstructed (001) surface. The chemistry of the above-described tetrahedral VO_x species has been studied in Ref. [38], by examining the interaction of NH_3 both with the Bronsted acid sites formed by the monomer hydroxyl groups, and with the Lewis acid sites, formed by the tetrahedral V ions. It was found that the interaction is rather weak (~0.7 eV in both cases, and that, contrary to previous conjectures, the monomer species are *not* able to protonate ammonia. The NO

[2] This feature makes our models differ from other ones based on tetrahedral vanadia units [40,41].

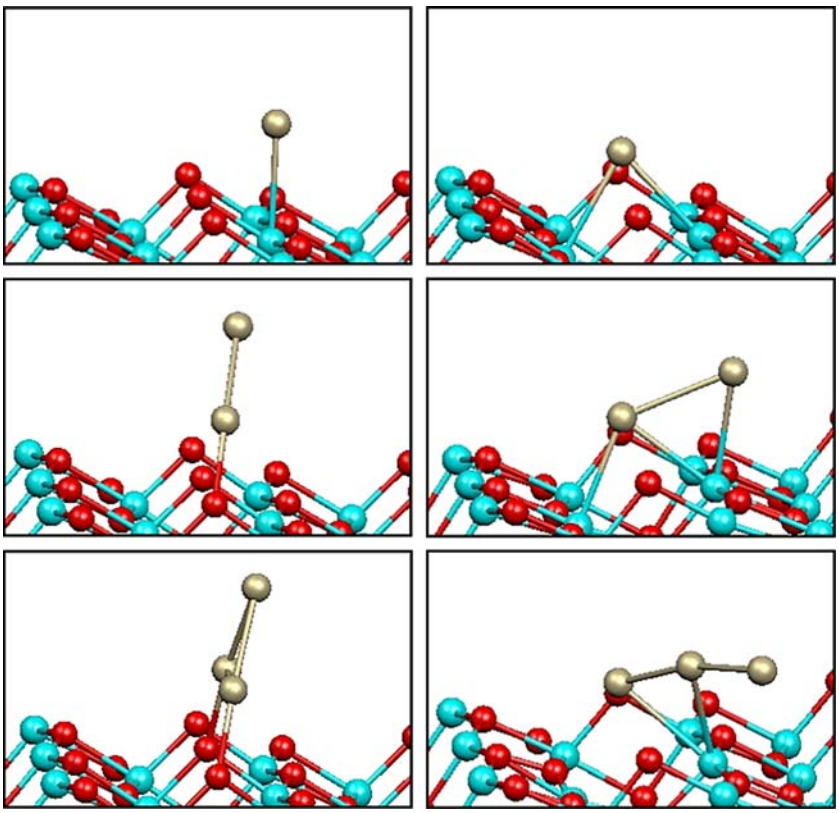

Fig. 4 Atomic configurations corresponding to the adsorption minima for small gold clusters on the (101) surface. Structures on the *right column* show the effect of the introduction of an oxygen vacancy (after Ref. [23])

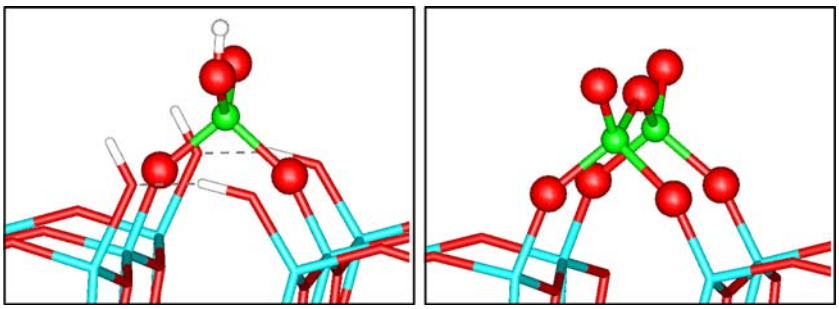

Fig. 5 Atomic configurations of the most favored VO_x species produced by the reaction of a vanadate precursor with the surface hydroxyls of the (001) surface (after Ref. [37])

selective catalytic reduction by NH_3 was also investigated. Mechanisms involving V-bonded and OH-bonded NH_3 species were considered, and in both cases activation energies compatible with the experimental ones were found. These results suggest that many channels may contribute to the NO reduction process.

The hypothesis that vanadia–titania coherent interfaces could be formed dates back to the 1970s [39], and has inspired several theoretical models [40,42–44]. In a recent experiment, Gao et al. [45] observed that VO_2 can actually grow pseudomorphically on the (001) anatase surface for several monolayers, with the uppermost layer being oxidized and $c(4 \times 4)$-reconstructed. To get insight into these findings, we performed calculations on slab models consisting of 1–3 layers of VO_x on a six layer $TiO_2(001)$ support. The inner VO_x layers were represented by pseudomorphic VO_2, whereas the topmost layer was allowed to assume a variable oxidation state. Among several possibilities, the structural models shown in Fig. 6 were selected. These can be obtained from the reduced pseudomorphic VO_x layer by adding oxygen atoms, or by removing V atoms. The formation energies of the films from bulk-V_2O_5 and from gaseous O_2 reservoirs have been evaluated using Eq. (1).

$$\Delta G(T,p) \approx \frac{1}{A}\left[E_{\mathrm{V}_n\mathrm{O}_m/\mathrm{TiO}_2} - E_{\mathrm{TiO}_2(001)} - \frac{n}{2}E^{\mathrm{bulk}}_{\alpha\text{-}\mathrm{V}_2\mathrm{O}_5} - \left(m - \frac{5}{2}n\right)\Delta\mu_{\mathrm{O}}(T,p)\right] \quad (1)$$

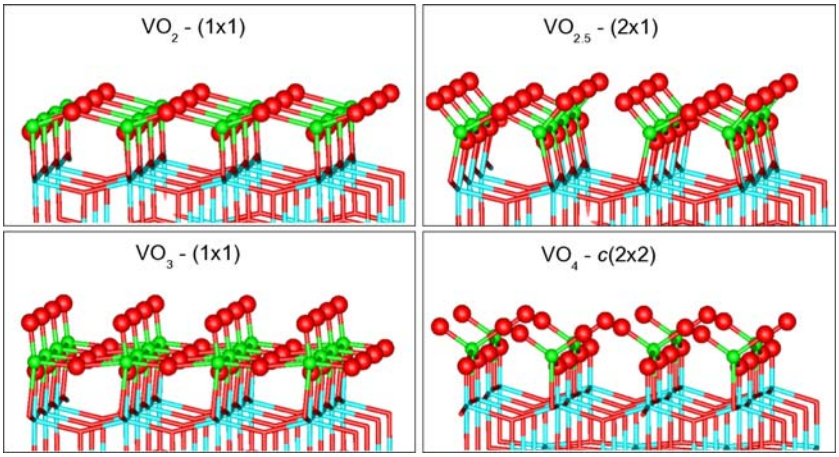

Fig. 6 Sketches of VO_x monolayers of increasingly oxidized state on the anatase (001) surface

where $E_{V_nO_m/TiO_2}$ is the total energy of the model, $E_{TiO_2(001)}$ is the total energy of support corrected by the (1×4) reconstruction energy, $E^{bulk}_{\alpha\text{-}V_2O_5}$ is the total energy per stoichiometric unit of α-V_2O_5, and A is the surface area of the model. The $\Delta\mu_O(T,p)$ parameter can be varied so as to simulate the effect of reducing/oxidising environments, and can eventually be used to make contact with the macroscopic (T and P) physical parameters (see, e.g., Ref. [46]). The origin of the $\Delta\mu_O(T,p)$ scale has been arbitrarily set to $\frac{1}{2}E_{O_2}$. Results, reported in Fig. 7, show that (i) The formation of pseudomorphic VO_2 multilayer films on anatase (001) supports is indeed favored; (ii) On increasing the thickness of the VO_2 film, terminating layers of increasing oxidation state are favored, so to keep the overall film stoichiometry close to V_2O_5; (iii) On the 3-ML film (which is the most thick taken in consideration), the over-oxidized terminal layer yields a $c(2 \times 2)$ reconstruction, in agreement with the experiment [45].

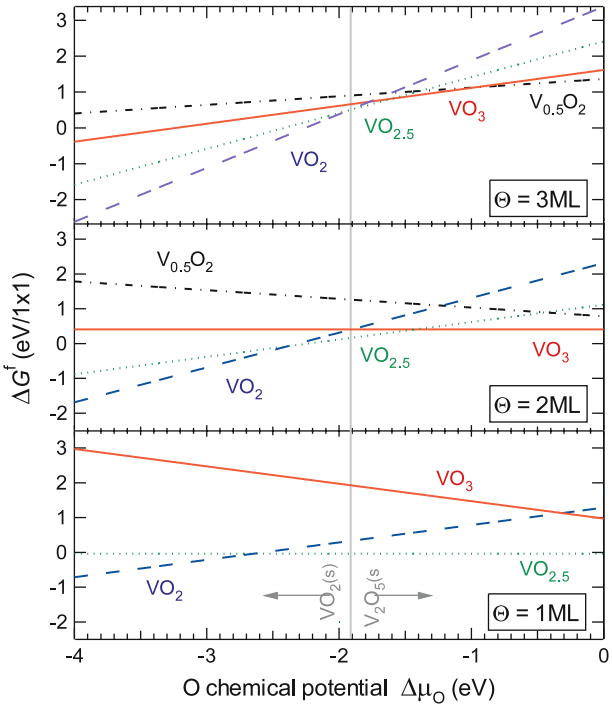

Fig. 7 Stability diagram for 1-ML (*bottom*), 2-ML (*middle*), and 3-ML (*top*) VO_x films supported on anatase (001). Films are made of $n-1$ inner layers of pseudomorphic VO_2, and terminated by a layer of variable stoichiometry as shown in Fig. 6. The *vertical gray bar* indicates the theoretical boundary between the stability zones of α-V_2O_5 and the R-VO_2 phases

6 Anatase nanosheets

Zhang and Banfield [47] observed that the synthesis of titania nanocrystals mainly results in the anatase phase, which on coarsening transformed to rutile. Rutile was in turn determined to be the stable TiO_2 bulk phase by Ranade et al. [2]. These results can be explained by the smaller average surface energy of anatase vs. rutile crystals, which could invert the small (2.61 kJ/mol [2]) stability difference between the two bulk phases [9]. However, the fact that anatase nanocrystals start forming from the very beginning of TiO_2 growth, when a kinetic control should be active, seems to indicate that the anatase formation is not only driven by thermodynamics. In fact, not long ago it was observed [48] that two-dimensional crystallites ("nanosheets") of titanium oxide can be prepared by delaminating a layered titanate. These nanolayers have a lepidocrocite-type structure, and a $Ti_{0.91}O_2$ formula. DFT calculations by Sato et al. [49], performed on a stoichiometric lepidocrocite model, proved that this structure is indeed remarkably stable (only 0.4 eV/TiO_2 over bulk anatase), and is characterized by a wide (3.15 eV) band gap.

Besides having a fundamental and a technological relevance, titania nanosheets are interesting because their

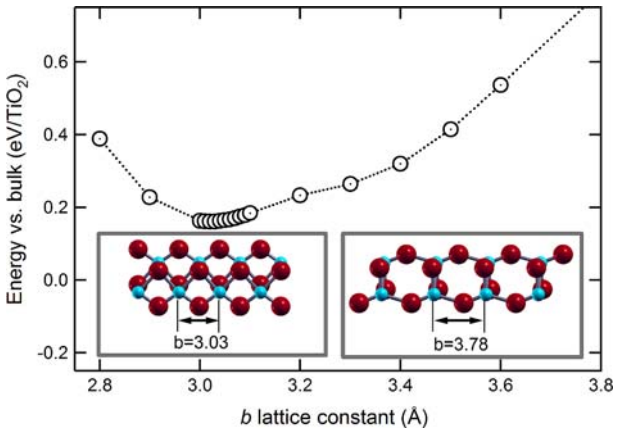

Fig. 8 Total-energy curve obtained by varying the *b* surface lattice constant (oriented along [100]) of a (001)-type anatase thin film. The *a* constant is frozen to the bulk value. Shown in insets are lateral views of the structure corresponding to the bulk (*right* $a = 3.78$ Å, $b = 3.78$ Å) and to the fully optimized (*left* $a = 3.79$ Å, $b = 3.03$ Å) lattice constants

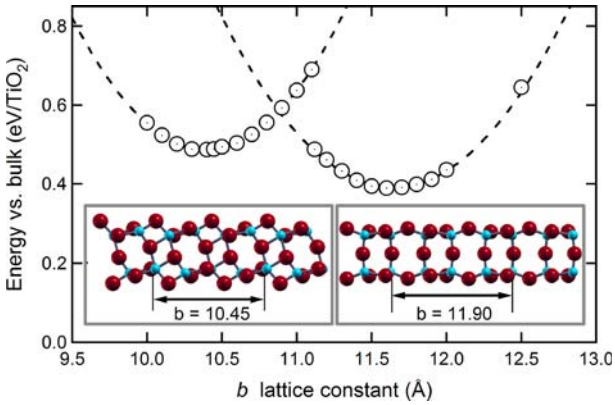

Fig. 9 Total-energy curve obtained by varying the *b* surface lattice constant (oriented along $[10\bar{1}]$) of a (101)-type anatase thin film. The *a* constant is frozen to the bulk value. *Dashed lines* are obtained by polynomial interpolation of the points corresponding to bulk-like films (on the *left*) and to minimum-like films (on the *right*). *Insets* are side views of the structures corresponding to the bulk (*left* $a = 3.78$ Å, $b = 10.45$ Å), and to the optimized film constants (*right* $a = 3.68$ Å, $b = 11.90$ Å)

stability can provide hints to understand the mechanisms favoring the formation of anatase in the initial stages of TiO_2 growth. In fact, we have found that if we take a two Ti-layers thick anatase film oriented in the (001) direction, and perform a systematic variation of one of the lattice constants, we obtain a new structure, as indicated by the total energy curve reported in Fig. 8. There is apparently no barrier for the transformation from a (001)-oriented anatase thin film into the lepidocrocite one: the two structures can be smoothly interconverted by letting the upper half of the film glide along [100] over the lower half. In other words, the two structures are closely connected. The high stability of the lepidocrocite film suggests that this could somehow be involved in the initial stages of TiO_2 growth. Then, the close relationship between the structures of lepidocrocite and anatase thin films could favor the latter over rutile when the crystallites turn to a three-dimensional form [Vittadini A, Casarin M (2006), to be published]. The formation of anatase nanorods starting from TiO_2 nanotubes (which are obtained by rolling TiO_2 nanosheets) has been indeed recently observed under hydrothermal conditions [50].

Interestingly, the lepidocrocite form is not the only titanium oxide nanosheet that can be obtained starting from anatase thin films. We have very recently found [Vittadini A, Casarin M (2006), to be published] that, if we take a two-layer thick, (101)-oriented anatase film, and we change the long lattice parameter *b* of the cell,[3] we obtain a new structure as indicated by the energy curve reported in Fig. 9. It should be noted that, at variance to the previously examined case, a barrier is present for the interconversion, because in this case some bonds have to be broken (the central O atoms of the film must turn from threefold to twofold coordinated). Furthermore, whereas the lepidocrocite sheet is obtained by a *compression* of the unit cell of the (001) thin film, the (101) thin film is stabilized by an *expansion* of the unit cell. To our knowledge, the structure of this nanosheet was never described before, and is rather interesting, as it bears some resemblance to V_2O_5: all the Ti atoms are in a fivefold coordinated environment, and most oxygens are twofold coordinated. Its formation seems to follow opposite criteria with respect to those favoring the formation of the previously examined lepidocrocite-type film, where the final structure is denser, and all ions tend to increase their coordination number.

The optimized lattice constants for the above-described nanosheets are $a = 3.79$ Å, $b = 3.03$ Å for the lepidocrocite-type and $a = 3.68$ Å, $b = 11.90$ Å for the (101)-derived one. Interestingly, ultra-thin films with very similar lattice constants, and with scanning tunneling maps compatible with the corresponding, above-described atomic structures, have been observed in titania films grown on Pt supports [51]. In particular, a commensurate phase is obtained on Pt(110), which is characterized by a coincidence structure having a periodicity of 14 lattice constants along $[1\bar{1}0]$. The properties of this phase are very well described by a model consisting of 14 Pt(110) unit cells and 13 TiO_2 lepidocrocite unit cells (repeated along the *b* direction) which is reported

[3] We make here reference to the rectangular unit cell, not the primitive one, which is rhombohedral.

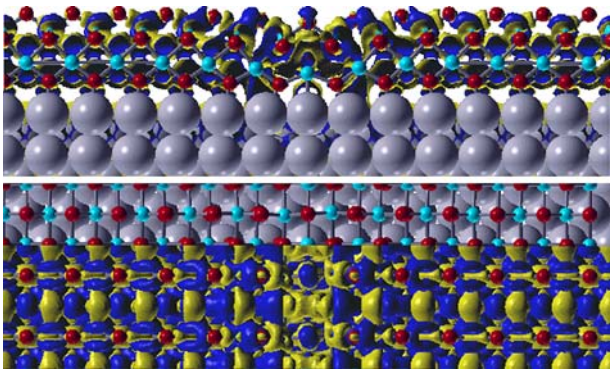

Fig. 10 Two views of a ball model of a (14 × 1) structure made by placing a TiO_2 lepidocrocite nanosheet on a Pt(110) surface. Note the rumpling, originated by the different periodicities of the overlayer and of the support. The *dark blue/yellow* surfaces correspond to regions of positive/negative electron difference density: note the electron transfer to the Ti cations

in Fig. 10, where the electron difference density is also shown.[4]

Overall, titania nanosheets appear to provide a unique possibility to get an atomic-level insight into the properties of nanoscale precursors of anatase, since the direct observation of the three-dimensional nanoclusters predicted by recent theoretical studies [52] is experimentally much more challenging.

7 Summary

After a decade of DFT investigations, the level of theoretical insight into the geometry, the stability, and the general adsorptive properties of the anatase surfaces is now close to that of the rutile ones. However, several challenges still remain, particularly (i) understanding the origin of the differences in the (photo)reactivity of the rutile and anatase polymorphs, (ii) explaining why the surfaces of rutile appear to be more easily reduced than those of anatase, (iii) clarifying the role of defects, e.g. steps, in the reactivity of anatase; (iv) modeling heterostructures where anatase is either the supporting or the supported phase, and predicting their catalytic properties, (v) elucidating the formation and growth mechanisms of anatase nanoparticles.

Acknowledgments The calculations described in Sect. 6 have been done with the Quantum Espresso package [7].

[4] The electron difference density of a composite system AB is given by $\Delta\rho_{AB}(\mathbf{r}) = \rho_{AB}(\mathbf{r}) - \rho_A(\mathbf{r}) - \rho_B(\mathbf{r})$, where the densities ρ refer to the composite system, and to the "fragment" systems, respectively.

References

1. Diebold U (2003) Surf Sci Rep 48:53
2. Ranade MR, Navrotski A, Zhang HZ, Banfield JF, Elder SH, Zaban A, Borse PH, Kulkarni SK, Doran GS, Whitfield HJ (2002) Proc Natl Acad Sci 99:6481
3. Hagfelt A, Grätzel M (1995) Chem Rev 95:49
4. Hadjivanov KI, Klissurski DG (1996) Chem Soc Rev 25:61
5. Madey TE (1999) Faraday Discuss 114:461
6. Car R, Parrinello M (1985) Phys Rev Lett 55:2471
7. Baroni S, dal Corso A, de Gironcoli S, Giannozzi P, Cavazzoni C, Ballabio G, Scandolo S, Chiarotti C, Focher P, Pasquarello A, Laasonen K, Trave A, Car R, Marzari N, Kokalj A, http://www.pwscf.org/
8. Vanderbilt D (1990) Phys Rev B 41:7892
9. Lazzeri M, Vittadini A, Selloni A (2001) Phys Rev B 63:155409
10. Beltrán A, Sambrano JR, Calatayud M, Sensato FR, Andrés J (2001) Surf Sci 490:216
11. Barnard AS, Zapol P (2004) Phys Rev B 70:235403
12. Wulff G (1901) Z Kristallogr Mineral 34:449
13. Diebold U, Ruzycki N, Herman GS, Selloni A (2003) Catal Today 85:93
14. Vittadini A, Selloni A, Rotzinger FP, Grätzel M (1998) Phys Rev Lett 81:2954
15. Arrouvel C, Digne M, Breysse N, Toulhoat H, Taybaud P (2004) J Catal 222:152
16. Barnard AS, Zapol P, Curtiss LA (2005) J Chem Theory Comput 1:107
17. Selloni A, Lazzeri M (2001) Phys Rev Lett 87:266105
18. Vittadini A, Selloni A, Rotzinger FP, Grätzel M (2000) J Phys Chem B 104:1300
19. Nilsing M, Lunell S, Persson P, Ojamäe L (2005) Surf Sci 582:49
20. Nilsing M, Persson P, Ojamäe L (2005) Chem Phys Lett 415:375
21. Gong X-Q, Selloni A, Vittadini A (2006) J Phys Chem B 110:2804
22. Selloni A., Vittadini A, Grätzel M (1998) Surf Sci 402–404:219
23. Vittadini A, Selloni A (2002) J Chem Phys 117:353
24. Tilocca A, Selloni A (2004) J Phys Chem B 108:19314
25. Vittadini A, Casarin M, Sambi M, Selloni A (2005) J Phys Chem B 109:21776
26. Aue DH, Bowers MT (1979) Stabilities of positive ions from equilibrium gas-phase basicity measurements. In: Bowers MT (ed) Gas phase ion chemistry, vol 2. Academic, New York, p.1
27. Herman GS, Donhàlec Z, Ruzycki N, Diebold U J Phys Chem B 107:2788
28. Tilocca A, Selloni A (2003) J Chem Phys 119:7445
29. Tanner RE, Sasahara A, Liang Y, Altman EI, Onishi H (2002) J Phys Chem B 106:8211
30. Han Y, Liu CJ, Ge Q (2006) J Phys Chem B 110:7463
31. Busca G, Lietti L, Ramis G, Berti F (1998) Appl Catal B Environ 18:1
32. Grzybowska-Świerkosz B (1997) Appl Catal A Gen 157:263
33. Forzatti P, Tronconi E, Elmi AS, Busca G (1997) Appl Catal A Gen 157:87
34. Bond GC (1997) Appl Catal A Gen 157:91
35. Bond GC, Perez Zurita J, Flamerz S, Gellings PJ, Bosch H, Van Ommen JG, Kip BJ (1996) Appl Catal 22:361
36. Anstrom M, Dumesic JA, Topsøe NY (2002) Catal Lett 78:281
37. Vittadini A, Selloni A (2004) J Phys Chem B 108:7337
38. Vittadini A, Casarin M, Selloni A (2005) J Phys Chem B 109:1652
39. Vejux A, Courtine P (1978) J Solid State Chem 23:93

40. Ferreira ML, Volpe M (2000) J Mol Catal A Chem 164:281
41. Khaliullin RZ, Bell AT (2002) J Phys Chem B 106:7832
42. Kachurovskaya KA, Mikheeva EP, Zhidomirov GM (2002) J Mol Catal A Chem 178:191
43. Calatayud M, Mguig B, Minot C (2003) Surf Sci 596:297
44. Sayle DC, Catlow CRA, Perrin MA, Nortier PJ (1996) J Phys Chem 100:8940
45. Gao W, Wang CM, Wang HQ, Henrich VE, Altman EI, De Gryse R (2004) Surf Sci 559:201
46. Reuter K, Scheffler M (2003) Phys Rev B 68:045407
47. Zhang HZ, Banfield JF (1998) J Mater Chem 8:2073
48. Sasaki T, Watanabe M, Hashizume H, Yamada H, Nakazawa H (1996) J Am Chem Soc 118:8329
49. Sato H, Ono K, Sasaki T, Yamagishi A (2003) J Phys Chem B 107:9824
50. Nian JN, Teng HS (2006) J Phys Chem B 110:4193
51. Orzali T, Casarin M, Granozzi G, Sambi M, Vittadini A (2006) Phys Rev Lett 97:156101
52. Harnad S, Catlow CRA, Woodley SM, Lago S, Mejias JA (2005). J Phys Chem B 109:15741